Residues Responsible for the Asymmetric Function of the Nucleotide Binding Domains of Multidrug Resistance Protein 1[†]

Lei Qin, Jimin Zheng, Caroline E. Grant, Zongchao Jia, Susan P. C. Cole, and Roger G. Deeley*

Division of Cancer Biology and Genetics, Cancer Research Institute, Departments of Biochemistry, Pathology and Molecular Medicine, Queen's University, Kingston, Ontario K7L 3N6, Canada

Received August 13, 2008; Revised Manuscript Received November 13, 2008

ABSTRACT: The two nucleotide binding domains (NBDs) of ATP binding cassette (ABC) transporters dimerize to form composite nucleotide binding sites (NBSs) each containing Walker A and B motifs from one domain and the ABC "C" signature from the other. In many ABC proteins, the NBSs are thought to be functionally equivalent. However, this is not the case for ABCC proteins, such as MRP1, in which NBS1 containing the Walker A and B motifs from the N-proximal NBD1 typically binds ATP with high affinity but has low hydrolytic activity, while the reverse is true of NBS2. A notable feature of NBD1 of the ABCC proteins is the lack of a catalytic Glu residue following the core Walker B motif. In multidrug resistance protein (MRP) 1, this residue is Asp (D793). Previously, we demonstrated that mutation of D793 to Glu was sufficient to increase ATP hydrolysis at NBS1, but paradoxically, transport activity decreased by 50−70% as a result of tight binding of ADP at the mutated NBS1. Here, we identify two atypical amino acids in NBD1 that contribute to the retention of ADP. We found that conversion of Trp653 to Tyr and/or Pro794 to Ala enhanced transport activity of the D793E mutant and the release of ADP from NBS1. Moreover, introduction of the P794A mutation into wild-type MRP1 increased transport of leukotriene C_4 approximately 2-fold. Molecular dynamic simulations revealed that, while the D793E mutation increased hydrolysis of ATP, the presence of the adjacent Pro794, rather than the more typical Ala, decreased flexibility of the region linking Walker B and the D-loop, markedly diminishing the rate of release of Mg^{2+} and ADP. Overall, these results suggest that the rate of release of ADP by NBD1 in the D793E background may be the rate-limiting step in the transport cycle of MRP1.

Multidrug resistance protein (MRP)[1] 1 confers resistance to a wide range of clinically important drugs, including many natural product-type anticancer agents (*1, 2*). Since the cloning of MRP1 from the multidrug-resistant human, small-cell lung cancer cell line, H69AR, eight additional human homologues have been identified (*3*−*8*). These proteins, together with the cystic fibrosis transmembrane conductance regulator (CFTR) and the sulfonylurea receptors (SURs) 1 and 2, comprise the "C" branch of the ATP binding cassette (ABC) superfamily of proteins. The ABCC proteins are distinguished from other ABC transporters by their relatively low ATPase activities and various structural features of their nucleotide binding domains (NBDs) (*3, 9*−*14*).

A fundamental feature of all ABC transporters is the presence of two NBDs that function cooperatively to bind and hydrolyze ATP. In prokaryotic transporters, the NBDs are typically structurally identical and in some so-called, "full-length" eukaryotic transporters, such as P-glycoprotein (P-gp, ABCB1), the NBDs are highly conserved and interchangeable (*15, 16*). The available crystal structures of a number of prokaryotic and eukaryotic ABC NBDs reveal a common arrangement of α-helices and β-sheets that form an L-shaped structure with an F1-like ATP binding arm containing the conserved Walker A and Walker B motifs, while the other arm contains the signature C sequence that distinguishes ABC NBDs from other ATPases (*17, 18*). The crystal structures of Rad50, BtuCD, MJ0796, MalK, HlyB, and, most recently, Sav1866 have demonstrated that two ABC NBDs dimerize to form a functional ATPase with two composite nucleotide binding sites (NBSs), each of which contains the Walker A and B motif of one NBD and the signature C sequence of the other (*19*−*24*). Studies of bacterial ABC transporters and proteins in which the NBDs are functionally interchangeable, such as P-gp, support a model in which the NBSs function stochastically in binding and hydrolysis of ATP (*25*). However, this model does not readily accommodate experimental data derived from studies of ABCC proteins. The NBSs of these proteins are clearly not functionally equivalent nor are their NBDs interchangeable, as in the case of P-gp. We and others have demonstrated that, in MRP1, NBS1, which contains the Walker A and B motifs of the N-proximal NBD1 and the atypical signature

[†] This work was supported by a grant from the Canadian Institutes of Health Research (MOP-62824). S.P.C.C. is a Canada Research Chair in Cancer Biology and Bracken Chair in Genetics and Molecular Medicine.

* To whom correspondence should be addressed. Tel: 613-533-6626. Fax: 613-533-6830. E-mail: deeleyr@queensu.ca.

[1] Abbreviations: MRP, multidrug resistance protein; NBD, nucleotide binding domain; MSD, membrane-spanning domain; SUR, sulfonylurea receptor; ATP-γ-S, adenosine 5′-*O*-(thiotriphosphate); AMP-PNP, adenosine 5′-(β,γ-imidotriphosphate); ABC, ATP-binding cassette; LTC_4, cysteine leukotriene C_4; PAGE, polyacrylamide gel electrophoresis; P-gp, P-glycoprotein; mAb, monoclonal antibody; β-gus, β-glucuronidase.

10.1021/bi801532g CCC: $40.75
Published on Web 12/08/2008

C sequence from NBD2, binds ATP with relatively high affinity but has very low hydrolytic activity, while the reverse is true of NBS2 (*9*−*11*).

In the majority of ABC NBDs, the residue immediately following the core Walker B motif is Glu, the carboxylate side chain of which is involved in hydrolysis of the β-phosphodiester bond of ATP. However, in NBD1 of the ABCC proteins this residue is not conserved. In most ABCC proteins, the residue following the Walker B is nonacidic, but in NBD1 of MRP1 it is an Asp residue (D793). Previously, we converted D793 to Glu in the expectation that hydrolysis of ATP would be enhanced at NBS1, resulting in increased transport activity (*26*). Although the mutation enhanced the conversion of ATP to ADP by NBS1 as expected, the overall rate of hydrolysis, as reflected by transport activity, decreased markedly. Photolabeling studies with azido-ATP and -ADP indicated that this was attributable to a decrease in the ability to release ADP from NBS1. We also showed that the presence of the tightly bound ADP at NBS1 strongly inhibited transition of the protein from high- to low-affinity substrate binding states, thus explaining the decrease in transport activity (*26*).

To determine why ADP release was impaired in the D793E mutant and to gain additional insight into the role of NBS1 in the transport cycle, we have examined the effects of replacing other variant amino acid residues in NBD1 with the corresponding amino acids present in NBD2. These studies show that conversion of Trp653 to Tyr and/or Pro794 to Ala is sufficient to restore ADP release by the D793E mutant and to increase LTC_4 transport activity to the level of the wild-type (wt) protein. LTC_4 binding of these mutant proteins was also studied in the absence or presence of nucleotides to confirm whether or not the release of ADP by NBD1 restored the ability of MRP1 to switch from a high- to low-affinity LTC_4 binding state.

Molecular modeling of an NBD1/2 dimer, based on the recently published crystal structure of NBD1 of MRP1 (*27*), combined with molecular dynamics simulations, revealed that introduction of the P794A mutation increases flexibility of the linker region between the Walker B motif and D-loop. This, in turn, markedly changes the dynamics of ADP binding at NBS1 and enhances the release of Mg^{2+} and nucleotide. Thus, the modeling and simulation results provide a possible mechanistic explanation for the ability of the P794A mutation to restore catalytic activity to the D793E mutation and to enhance activity of the wt protein. These results are also consistent with the possibility that the release of ADP from NBS1 of MRP1 and possibly other ABCC proteins may be the limiting step in the catalytic cycle.

MATERIALS AND METHODS

Materials. [14,15,19,20-^{3}H]LTC_4 (150 Ci/mmol) was purchased from Perkin-Elmer Life Sciences Inc. (Boston, MA). LTC_4 was purchased from Calbiochem (La Jolla, CA). 8-Azido-[γ-^{32}P]ATP and 8-azido-[α-^{32}P]ATP (specific activity 10−20 Ci mmol^{-1}) were purchased from Affinity Labeling Technologies Inc. (Lexington, KY). Magnesium chloride, EDTA, EGTA, beryllium fluoride, sodium orthovanadate, AMP, ATP, AMP-PNP, and ATP-γ-S were purchased from Sigma-Aldrich (St. Louis, MO). Fluorographic reagent Amplify NAMP100 and anti-mouse and anti-rat IgG conjugated with horseradish peroxidase were purchased from GE Healthcare (Piscataway, NJ). Chemiluminescent substrate for immunoblotting was from Perkin-Elmer Life Sciences Inc. (Boston, MA).

Multialignment and Hidden Markov Model (HMM) Analysis of the Amino Acid Sequences of NBDs of ABC Transporters. The amino acid sequences of NBDs from ABCC proteins and various other ABC transporters were aligned using Clustal W (*28*), and the multialignment was analyzed with HMM-build to create an HMMER2.0 file (*29*). Finally, the HMMER2.0 file was processed using LogoMat-M to visualize the result of HMM analysis (*30*).

Generation of MRP1 Mutants. DNA fragments encoding amino acids 1−932 and 932−1531 of human MRP1 were originally cloned into pFastBac Dual vector (Invitrogen Corp., Carlsbad, CA) as described (*9, 31*), and the construct was designated dual-halves (dh) MRP1. The dh MRP1 construct containing the D793E mutation was also constructed previously and designated dh D793E (*26*). Additional mutations (W653Y, V680T, P794A, V1432G, L1437R, and C1439S) were introduced into the dh D793E vector by site-directed mutagenesis using a QuikChange II kit (Stratagene, La Jolla, CA). The forward primers for W653Y, V680T, P794A, V1432G, L1437R, and C1439S were 5′-GCCACATTCACCTATGCCAGGAGC-GAC-3′, 5′-GTGGTGGGCCAGACGGGCTGCGGAAAG-3′, 5′-TTTA-CCTTCGATGAGGCCCTCTCAGCAGTGGA-3′, 5′-AGAAC-CTCAGTGGCGGGCAGCGC-3′, and 5′-CAGCGCCAGC-GTGTGAGCCTAGCCCG-3′, respectively. DNA sequences of reverse mutation primers were the reverse complementary sequences of the forward primers. Briefly, to make W653Y, V680T, and P794A mutations, a *Bam*HI−*Xba*I fragment from the dh D793E construct was cloned into pBluescript II KS (+) vector (Fermentas International Inc., Burlington, Ontario, Canada), and mutagenesis PCR reactions were performed according to the manufacturer's manual. The presence of the mutation was confirmed by DNA sequencing (ACGT Corp., Toronto, Ontario, Canada). The isolated *Bsu*36I−*Xba*I fragment containing the mutation was used to replace the same region in the pFBdh D793E vector. To make V1432G, L1437R, and C1439S mutations, a *Kpn*I−*Cla*I MRP1 DNA fragment was cloned into pBluescript II KS vector, and PCR mutagenesis was performed as described above. Mutations were validated by sequencing (ACGT Corp., Toronto, Ontario, Canada) and cloned into the pFBdh D793E vector to replace the equivalent *Kpn*I−*Cla*I DNA sequence.

The P794A mutation was also created in wt MRP1. To do so, a *Bam*HI−*Xba*I DNA fragment was subcloned into pBluescript II KS (+) as a mutagenesis template. The forward primer for the P794A mutation was 5′-TACCTCT-TCGATGATGCCCTCTCAGCAGTGG-3′, and the reverse primer was its complement. The mutation was introduced by PCR mutagenesis, as above. The *Bsu*36I−*Xba*I fragment with the P794A mutation was cloned into pFBdh MRP1 to replace the equivalent DNA. The presence of the mutation and fidelity of the sequence were confirmed by sequencing.

Viral Infection and Membrane Vesicle Preparation. dh wt and mutant MRP1 DNAs cloned in pFastBac dual vectors were transformed into DH10Bac cells to yield recombinant bacmids, as described (*31, 32*). Infection of insect Sf21 cells and cell harvesting procedures were as described (*9, 31*). Membrane vesicles were prepared using nitrogen cavitation

and sucrose density gradient centrifugation and finally suspended in transport buffer (TB, 50 mM Tris-HCl, pH 7.4, 250 mM sucrose), as described (*33, 34*).

Immunoblotting of MRP1 Half-Molecules and LTC_4 Vesicle Transport Assays. Membrane vesicles containing similar amounts of wt and mutant MRP1 half-molecules were analyzed by SDS−PAGE. Proteins were then transferred to Immobilon-P membranes (Millipore Corp., Billerica, MA) and probed with mAbs MRPr1 (epitope aa 228−237) and MRPm6 (epitope aa 1511−1520), specific for the NH_2- and COOH-proximal halves of MRP1, respectively (*35, 36*). MRP1 fragments were detected using the Western Lightning kit (Perkin-Elmer Life Sciences Inc., Boston, MA), and the relative MRP1 expression levels were estimated by densitometry using a Fluorochem Imaging System (Alpha Innotech Corp., San Leandro, CA). Uptake of [^{3}H]LTC_4 (50 nM, 20 nCi) into membrane vesicles was measured at 23 °C in the presence of 4 mM AMP or ATP using a rapid filtration technique described previously (*33*).

Photolabeling of MRP1 NBDs with 8-Azido-[γ-^{32}P]ATP. Photolabeling of wt and mutant MRP1 with 8-azido-[γ-^{32}P]ATP was performed as described (*9*) with minor modifications. Briefly, membrane vesicles (20−30 μg of total protein) containing similar amounts of MRP1 were resuspended in ice-cold TB containing 5 mM $MgCl_2$ and 5 μM 8-azido-[γ-^{32}P]ATP. After 5 min on ice in a 96-well plate, samples were cross-linked (λ = 302 nm) for 8 min also on ice with a CL-1000 UV cross-linker (UVP, LLC, Upland, CA). Samples were then transferred into ice-cold stop buffer (500 μL, 50 mM Tris-HCl, pH 7.4, 0.1 mM EGTA, and 5 mM $MgCl_2$), recovered by centrifugation, and washed a second time. After the second wash, the pellets were suspended in 20 μL of Laemmli buffer containing 100 mM DTT. Proteins were separated by SDS−PAGE using a 7−20% gradient gel. Gels were dried and autoradiographed at −70 °C using Kodak BioMax MS films (Eastman Kodak Inc., Rochester, NY). In order to confirm the specificity of ATP binding, duplicate samples were incubated with 8-azido-[γ-^{32}P]ATP in the presence of a large excess of the slowly hydrolyzable ATP analogue, ATP-γ-S (500 μM).

Trapping of 8-Azido-[α-^{32}P]ATP by MRP1 NBDs in the Absence or Presence of Orthovanadate (VO_4) or Beryllium Fluoride (BeFx). To study the effect of mutations on ADP trapping by MRP1 NBDs, membrane vesicles (20−30 μg of total protein) were incubated in TB containing 5 mM $MgCl_2$ and 8-azido-[α-^{32}P]ATP (10 μM) at 37 °C for 15 min. The reaction was performed in the absence or presence of VO_4 (1 mM) or BeFx (200 μM) and stopped by addition of ice-cold stop buffer (500 μL), as described (*9, 26*). Unbound nucleotides were removed by two rounds of washing, as above. The pellets were then resuspended in stop buffer (15 μL), transferred to a 96-well plate on ice, and UV irradiated for 8 min as above. After addition of 4 × concentrated Laemmili buffer, proteins were separated by SDS−PAGE (7−20% gradient gel). The gel was then dried and autoradiographed at −70 °C as above.

Photoaffinity Labeling of MRP1 with [^{3}H]LTC_4. Photolabeling of the coexpressed N- and C-halves of MRP1 with [^{3}H]LTC_4 was carried out as described (*26, 37, 38*). To explore the relationship between nucleotide binding and trapping and LTC_4 binding, the assays were performed in the absence or presence of ATP (1 mM), AMP-PNP (4 mM), ATP-γ-S (4 mM), ATP and VO_4 (1 mM), or ATP and BeFx (200 μM). Briefly, Sf21 membrane vesicles (50 μg of total protein) were incubated with or without nucleotides in TB at 23 °C in a 96-well plate. After 20 min, [^{3}H]LTC_4 (200 nCi, 200 nm) was added, and the incubation was continued for another 20 min. Samples were then frozen using liquid N_2 and then UV cross-linked for 1 min (λ = 302 nM). The cycle of freezing and cross-linking was repeated a total of 10 times. Membrane proteins were then analyzed by SDS−PAGE using a 10% gel. The gel was first immersed in fixation buffer (25% 2-propanol, 65% water, and 10% acetic acid) at room temperature for 30 min and then soaked in Amplify NAMP100 for another 30 min before being dried. Dried gels were then autoradiographed at −70 °C.

Evaluation of the Effects of D793E and D793E/P794A Mutations by Molecular Modeling and Dynamic Simulation Analysis. To evaluate the impact of the D793E mutation on ATP hydrolysis at NBS1 and the influence of the D793E/P794A double mutation on ADP release, a MRP1 NBD1/NBD2 heterodimer model was constructed using the MJ0796 NBD dimer (PDB code 1L2T) as a template, based on a previously published method (*27*). First, the Mg^{2+}-ATP bound MRP1 NBD1 crystal structure (PDB code 2CBZ) was superimposed on one monomer of the MJ0796 homodimer. The MRP1 NBD2 was then modeled with the Swissprot server (*39, 40*) and positioned on the second monomer of MJ0796 dimer to generate the MRP1 NBD1-NBD2 heterodimeric structure. The critical motifs (Walker A, Walker B, Q-loop, and H-loop) were all found to adopt conformations similar to the original MJ0796 NBDs. With the available wt NBD dimer model, NBD1-D793E and NBD1-D793E/P794A mutants were generated using the Xtalview program (*41*). In subsequent steps, mutant MRP1 NBD1-NBD2 dimers were compared with the wt dimer by energy minimization and 40 ps molecular dynamics simulation in an aqueous phase, using identical parameter settings for wt and mutant models. Briefly, all energy minimizations were performed using 400 steps of the steepest descent algorithm. Equilibration was performed using harmonic restraints on the protein non-H atoms (H atom only present in ATP) (force constant = 1000 kJ·mol^{-1}·nm^{-2}), a Berendsen thermostat, and pressure maintained at 1 bar by a Berendsen barostat. The simulation process was run in the NPT ensemble at a temperature of 300 K. The particle mesh Ewald (PME) method was used to treat long-range electrostatics, and the single point charge (SPC) water model was used for the solvent. The integration time step was 2 femtosecond (fs), and coordinates were saved every 1 ps for subsequent analysis. The linear constraints solver (LINCS) algorithm for molecular simulations was used to restrain all bond lengths. GROMACS v.3.1 (*42*) molecular dynamics simulation package with the GROMOS96 force field was used for simulation and result analysis. Finally, three-dimensional graphics were produced using Pymol (*43*).

RESULTS

Conserved Nonidentical Amino Acids in Critical Regions of the Nucleotide Binding Domains (NBD) of ABCC Transporters. The two NBSs of ABCC transporters are known to function differently, with NBS1 typically displaying little or no hydrolytic activity (*44*). Conservation of these functional differences among members of the ABCC family prompted us to search for amino acids that were conserved

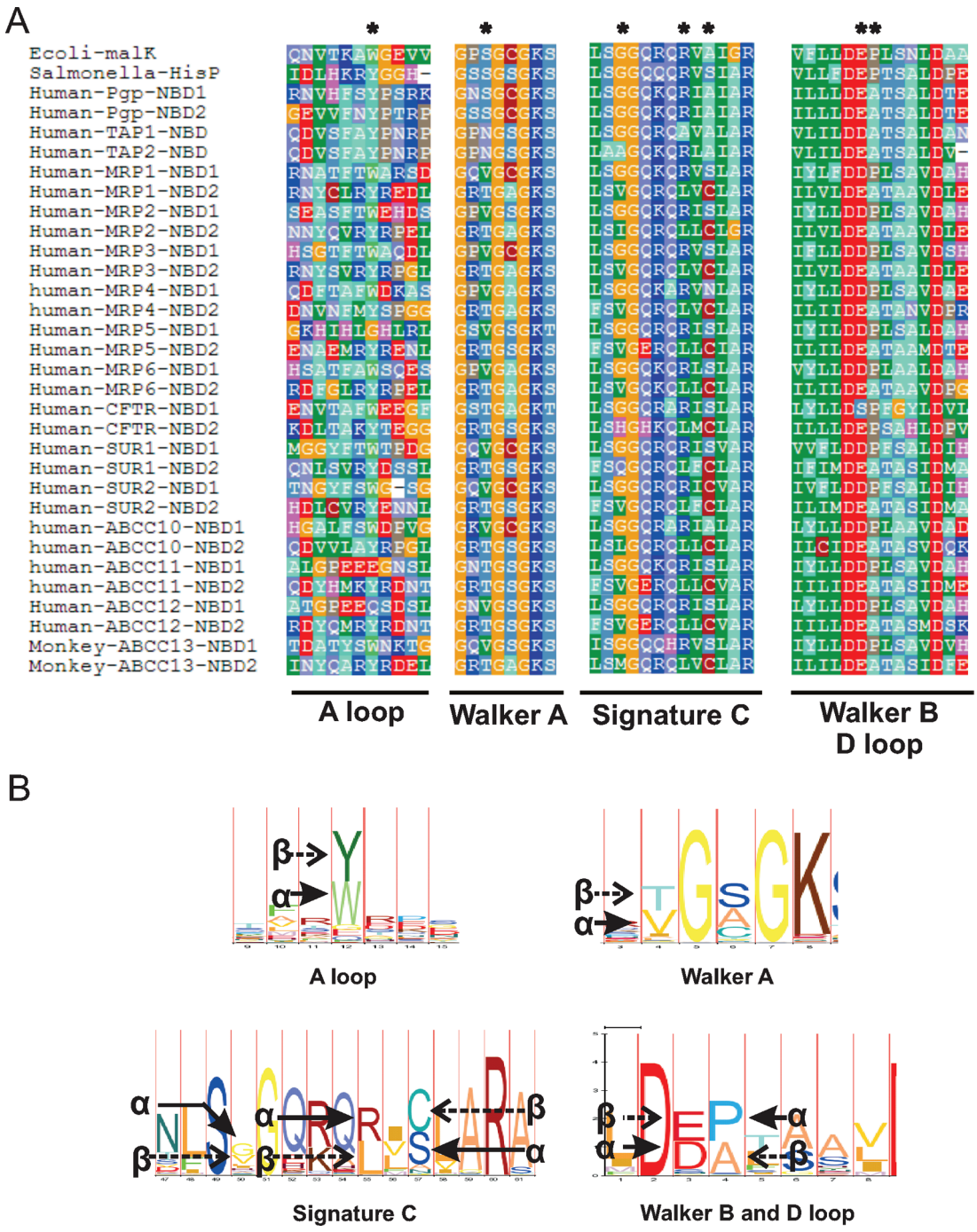

FIGURE 1: Asymmetric conserved residues present in the NBDs of the ABCC proteins. (A) Sequence alignment of the nucleotide binding domains (NBDs) of ABCC proteins and other more distantly related ABC transporters. The alignment was generated using Clustal W and with the exception of the HisP sequence was not subject to further manipulation. In the case of HisP, a minor adjustment was made manually to the alignment of the A-loop region so that the position of the conserved Tyr (marked with an asterisk) which interacts with nucleotide was consistent with the comparable aromatic residue in other proteins. Underlined regions of functional importance are the A-loop, Walker A, signature C, Walker B, and D-loop. Positions where conserved residues differ between NBD1 and NBD2 of the ABCC transporters are indicated by an ∗. (B) The asymmetric conservation of these residues is illustrated by HMM logos produced using hidden Markov model (HMM) algorithms. In each logo, the stack height is determined by the deviation of the position's letter emission frequencies from the background frequencies of the letters. At asymmetric positions, amino acids favored by NBD1 and NBD2 are indicated with α or *β*, respectively.

across family members but which differed between the two NBDs. Our previous studies focused on the identity of the amino acid following the generally conserved COOH-proximal Asp residue of the Walker B motif. This is typically a Glu but not in NBD1 of the ABCC proteins (or TAP1) where it is replaced by a nonacidic residue or, in the case of MRP1, by Asp (*26*). The multiprotein alignment shown in Figure 1A compares the two NBDs of the ABCC proteins with each other and with the NBDs of selected prokaryotic transporters, as well as eukaryotic transporters, such as P-glycoprotein, in which the two NBDs are structurally and functionally similar. Conserved residues that differ between NBD1 and NBD2 of the ABCC proteins are highlighted (Figure 1A). For example, the highly conserved Tyr found in the A-loop of both NBDs of P-gp and in NBD2 of ABCC proteins is a Trp in NBD1 of ABCC proteins. Similarly, the

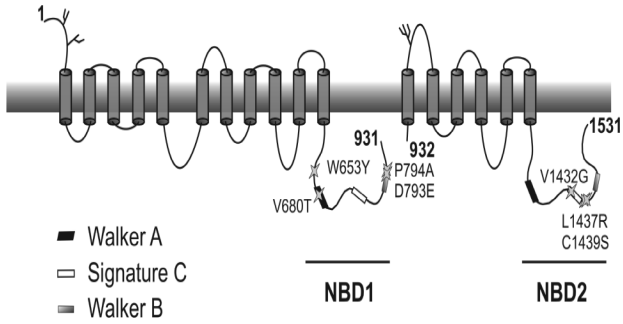

FIGURE 2: Topology of MRP1 showing the positions of conserved asymmetric mutations selected for mutation. Schematic diagram of the two MRP1 half-molecules encoded by the dual expression vectors described in the text, indicating the locations of conserved asymmetric amino acid residues selected for study based on the analysis presented in Figure 1, together with the identity of the mutations introduced.

residue immediately following what is usually the catalytic Glu residue COOH-proximal to Walker B is Ala in NBD2 and Pro in NBD1.

Figure 1B is a cartoon illustrating the relative conservation of nonidentical residues in critical, functional elements in each of the two ABCC NBDs, generated using the HMM algorithm. As can be seen from the figure, in addition to departures from the most common amino acids in the A-loop and the Walker motifs of NBD1, atypical amino acids are found at locations in the signature C sequence of NBD2. This is consistent with the atypical activity of NBD1 among the ABCC proteins and the established cooperativity among elements in one NBD with the C-signature of the opposing domain.

Dual Expression of wt and Mutant Halves of MRP1 in Sf21 Cells. As in previous studies, we used a baculovirus dual-expression system which allows reconstitution of a functional transporter from two half-molecules of the protein with approximately 90% efficiency (*9*). This system facilitates analyses of the effects of mutations on the function of each NBD. The conserved asymmetric residues in NBD1 and NBD2 that were mutated in the background of the previously described D793E mutation are shown in Figure 2, with each of the atypical residues being replaced by the corresponding amino acid from the other NBD. The levels of expression of each half of MRP1 were determined by immunoblotting and densitometry using mAbs MRPr1 and MRPm6 to detect the NH_2- and COOH-proximal halves of MRP1, respectively. All mutant constructs were expressed at levels between 70% and 130% of the respective wt half-molecule. Densitometry and comparison with full-length MRP1 also indicated that, as previously observed, expression of each half-molecule was approximately stoichiometrically equivalent within a single construct (Figure 3A,C).

Evaluation of LTC_4 Transport by Dual-Expressed Mutant and wt Halves of MRP1. As previously reported, the D793E mutation decreased ATP-dependent LTC_4 transport by 50−70% relative to the wt construct (*26*). Determination of the effects of the additional mutations revealed that two second mutations, P794A and W653Y, were each able to restore activity of the D793E mutant to levels that were comparable to or somewhat higher than wt MRP1. The Walker A V680T mutation and the signature C V1432G mutation in NBD2 were without effect, while the double L1437R/C1439S signature C mutation essentially inactivated the D793E protein (Figure 3B).

To investigate if the effects of the P794A and W653Y mutations on LTC_4 transport activity were additive, both mutations were introduced into the D793E mutant. Although LTC_4 transport activity was increased in the triple mutant relative to that of dh D793E, it was similar to that of wt dh MRP1 (Figure 3D). Thus the positive effect of the individual W653Y and P794A mutations on activity of the D793E mutant MRP1 was not additive to any detectable extent.

Effect of Mutations on ATP Binding by Each NBS. The photoactivatable ATP derivative 8-azido-[γ-^{32}P]ATP has been used extensively to assess the relative levels of ATP binding by ABC transporters. In MRP1, 8-azido-[γ-^{32}P]ATP has been shown to predominantly photolabel NBD1 under nonhydrolytic conditions (i.e., at 0−4 °C) (*9*). As found previously (*26*), the D793E mutation did not change the relative levels of photolabeling of either NBD (Figure 4). Overall, the effects of the additional mutations on the labeling profile of the D793E mutant were minimal with the possible exception of the W653Y mutation which modestly decreased the photolabeling of NBD1 relative to NBD2. In all cases, photolabeling of both NBDs was eliminated in the presence of a 100-fold molar excess of ATP-γ-S, indicating that the photolabeling observed was the result of specific binding of 8-azido-[γ-^{32}P]ATP.

Effect of Mutations on Trapping of 8-Azido-[α-^{32}P]ATP/ADP by Each NBD. Previously, we demonstrated that the D793E mutation markedly increased the extent of tight binding of ADP at NBS1 (*26*). Furthermore, the occlusion of ADP at NBS1 was to a large extent independent of the presence of VO_4, unlike the trapping of ADP observed at NBS2 of wt MRP1 and typically observed in studies of other ABC transporters (*9, 10, 45*). Consequently, we proposed that the decrease in LTC_4 transport activity of MRP1 D793E was attributable to tight VO_4-independent binding of ADP by the mutant NBS1 and a decrease in its rate of release (*26*). Concomitant with the tight binding of ADP at NBS1 by the D793E mutant protein, we observed a decrease in VO_4-dependent trapping of ADP at NBS2. This would be expected if, as proposed by the alternating site model of ATP hydrolysis of ABC transporters, both NBSs cannot exist contemporaneously in a posthydrolytic transition state (*46*).

The effect of the additional mutations described here on the trapping of 8-azido-[α-^{32}P]ATP under hydrolytic conditions in the presence and absence of VO_4 is shown in Figure 5. In addition, we also examined the effect of BeFx which, unlike VO_4, is believed to result in tight binding of ADP in a conformation resembling the ATP-binding ground state, rather than a posthydrolytic transition state (*45, 47, 48*). As observed previously, the predominant site of photolabeling of wt MRP1 under trapping conditions in the presence of either BeFx or VO_4 was NBS2, and very little photolabeling of either NBD was detected in the absence of BeFx or VO_4. The results also confirmed previous studies indicating that the D793E mutation resulted in VO_4-independent occlusion of nucleotide at NBS1 and that VO_4-dependent trapping at NBS2 was markedly decreased (*26*). In contrast, BeFx markedly increased the extent of trapping at both sites, particularly at NBS2, so that the photolabeling profile of the D793E mutant was similar to that obtained with the wt protein.

The D793E/V1432G mutation, which did not restore LTC_4 transport activity, displayed VO_4-independent photolabeling of NBD1 and a decrease in VO_4-dependent photolabeling of NBD2 relative to wt MRP1, as observed with the D793E

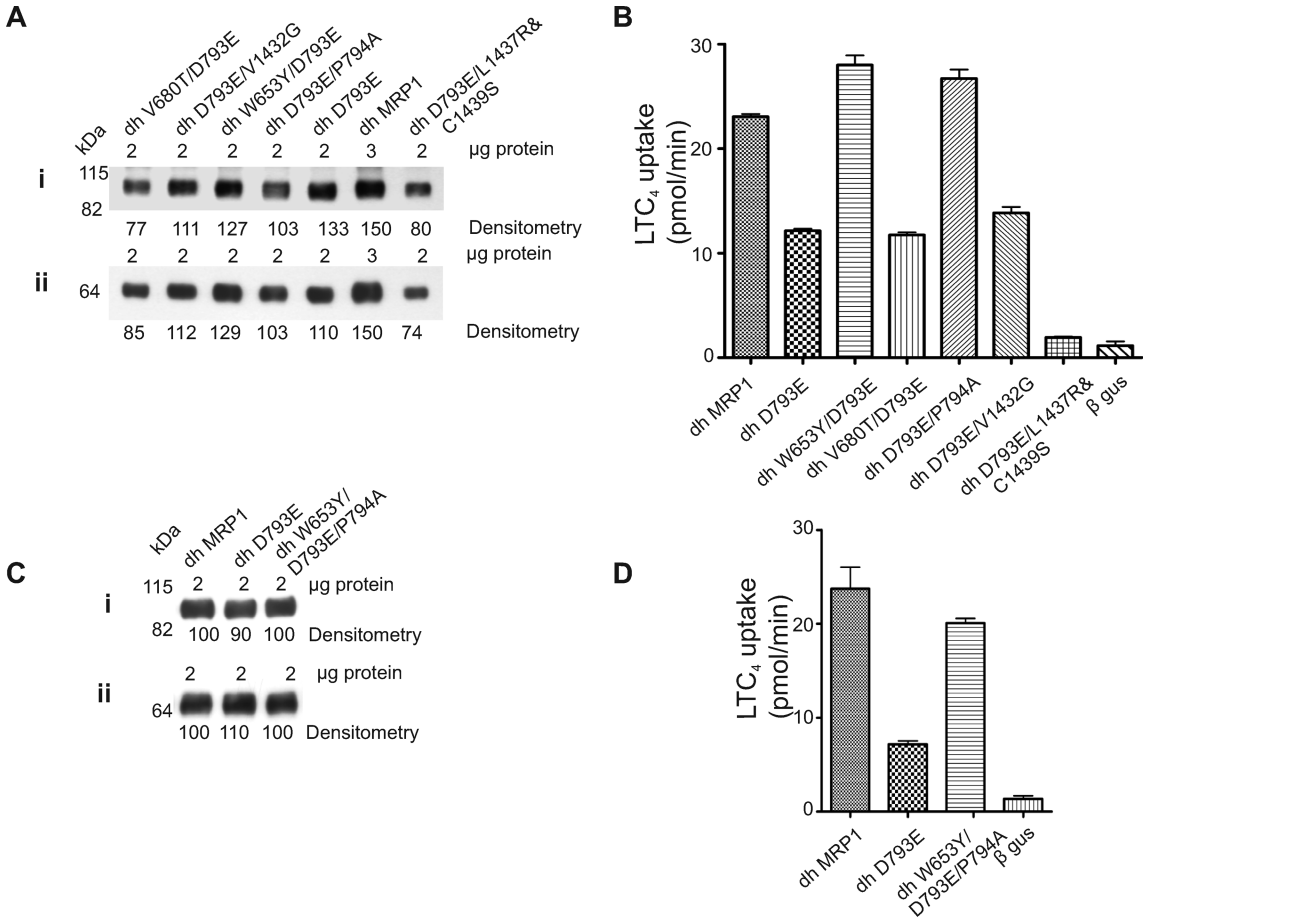

FIGURE 3: Expression of wt and mutant dual halves of MRP1 in Sf21 cells and determination of [^{3}H]LTC$_4$ transport activity. (A) Immunoblot of membrane vesicle proteins isolated from Sf21 cells expressing wt or mutant dual halves of MRP1 (dh D793E, dh W653Y/D793E, dh V680T/D793E, dh D793E/P794A, dh D793E/V1432G, and dh D793E/L1437R/C1439S) or Sf21 cells infected with a control vector expressing β-gus. (C) Immunoblots of the wt and mutant dual halves of MRP1 (dh D793E and dh W653Y/D793E/P794A). In both panels A and C, MRPr1 and MRPm6 mAbs were used to detect the NH$_2$-proximal (i) and COOH-proximal (ii) halves of MRP1 as described in Materials and Methods. The relative level of wt dh MRP1 indicated below the immunoblots in panel A was adjusted to 150% to compensate for differences in the amount of total membrane proteins from cells expressing wt dh MRP1 (3 μg) compared with the various mutants analyzed (2 μg). (B, D) ATP-dependent LTC$_4$ transport by membrane vesicles containing wt or mutant MRP1 was carried out at 23 °C for 1 min with membrane samples (2 μg) as described in Materials and Methods. Results shown are the mean ± SD of triplicate determinations from a typical experiment. [^{3}H]LTC$_4$ transport activity by MRP1 mutants was normalized to that of wt dh MRP1 based on the densitometry of immunoblots (panels A and C).

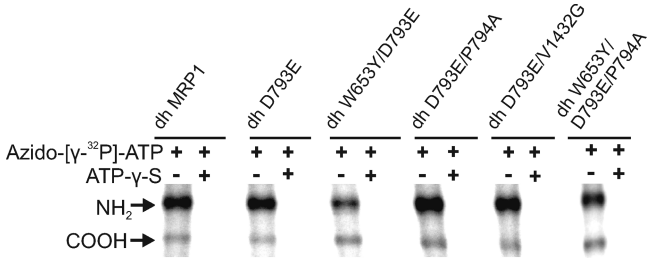

FIGURE 4: Photolabeling of wt and mutant dual halves of MRP1 by 8-azido-[γ-^{32}P]ATP. Photolabeling of membrane vesicle proteins (20−30 μg of total protein depending on the relative levels of expression of wt and mutant MRP1) from Sf21 cells expressing wt and mutant MRP1 half-molecules was performed at 4 °C using 5 μM 8-azido-[γ-^{32}P]ATP, in the absence or presence of 500 μM ATP-γ-S. Samples were photolabeled under UV light and washed twice with stop buffer to remove free nucleotides and then subjected to SDS−PAGE. Labeled proteins were detected by autoradiography, as described in Materials and Methods. NH$_2$ and COOH indicate the position of NH$_2$- and COOH-proximal halves of MRP1, the extent of photolabeling of which is indicative of 8-azido-[γ-^{32}P]ATP binding at NBS1 and NBS2, respectively.

single mutation (Figure 5). However, both second mutations that restored LTC$_4$ transport by D793E MRP1, W653Y and P794A, decreased VO$_4$-independent photolabeling of NBD1 and enhanced the extent of VO$_4$-dependent trapping at this site. The photolabeling profile of the all of the double mutants in the presence of BeFx was similar to the single D793E mutant and wt protein with NBD2 being the predominantly labeled site.

[^{3}H]LTC$_4$ Photolabeling of wt and Mutant Dual Halves of MRP1 in the Absence or Presence of ATP plus VO$_4$ or BeFx. In the absence of nucleotides, [^{3}H]LTC$_4$ binds to MRP1 with relatively high affinity and can be photo-cross-linked to the protein. Photo-cross-linking occurs predominantly to MSD1 with weaker cross-linking to MSD2 (*32, 37*). We have shown previously that the apparent affinity of wt MRP1 for LTC$_4$, as indicated by the efficiency of photolabeling, is decreased in the presence of ATP, as well as certain ATP analogues such as ATP-γ-S, and that the inhibitory effect of ATP on photolabeling is markedly enhanced in the presence of VO$_4$ or BeFx (*26, 38*). This decrease in apparent affinity for LTC$_4$ is presumed to reflect the transition from a high- to low-affinity substrate binding state following formation of a tightly closed NBD dimer (*38, 48*). One of the striking effects of the D793E mutation is that it prevents

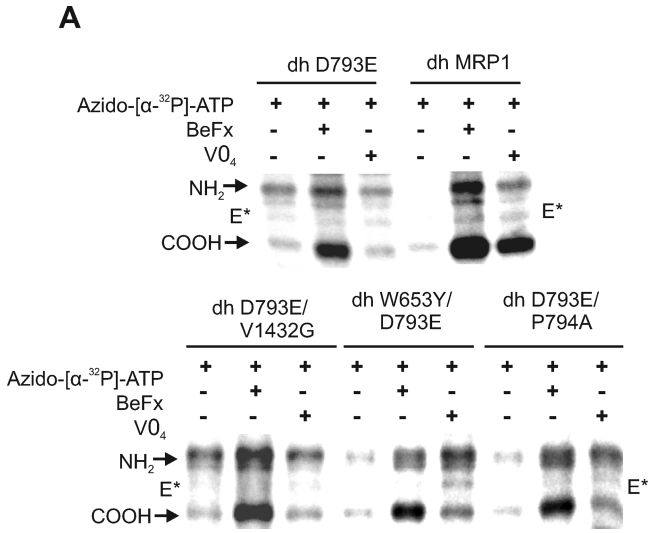

FIGURE 5: Photolabeling of wt and mutant MRP1 by 8-azido-[α-^{32}P]ATP under hydrolytic conditions. Nucleotide trapping assays were carried out by incubating membrane vesicles (20−30 μg of total protein depending on the relative levels of expression of wt and mutant MRP1) from SF21 cells with 8-azido-[α-^{32}P]ATP (10 μM) for 15 min at 37 °C with or without BeFx (200 μM) or VO_4 (1 mM). Samples were then processed as described in the legend to Figure 4. The positions of NH_2- and COOH-terminal halves of MRP1 are indicated by NH_2 and COOH, respectively. E* indicates the positions of photolabeled endogenous proteins.

the transition from high- to low-affinity LTC_4 binding states in the presence of ATP, regardless of whether or not VO_4 is also present (*26*). In view of the effects of the W653Y and P794A mutations on VO_4-dependent nucleotide trapping at NBS1, we examined their influence on the ability of MRP1 D793E to shift between high- and low-affinity conformations.

As previously observed, ATP in the presence of VO_4 markedly decreased LTC_4 photolabeling of wt MRP1 but had no effect on the apparent affinity of the D793E mutant (*26*) (Figure 6A). We have previously presented evidence that this is the result of tight VO_4-independent binding of ADP by the mutant NBS1 which appears to preclude formation of the low-affinity LTC_4 binding state (*26*). Consistent with their effects on VO_4-dependent nucleotide trapping by the D793E mutant protein (Figure 5), both the W653Y and P794D second mutations restored the ability of ATP plus VO_4 to induce the shift from high- to low-affinity LTC_4 binding (Figure 6A). The behavior of the triple mutant (Figure 6A) did not differ substantially from either of the two double mutations.

We also compared the effects of VO_4 with those observed with BeFx, given that the latter is thought to trap ADP in a conformation mimicking the ATP binding ground state. Like VO_4, BeFx was highly effective in shifting wt MRP1, as well as the double and triple mutant proteins, into a low-affinity conformation in the presence of ATP. However, in contrast to VO_4, BeFx plus ATP also markedly decreased LTC_4 photolabeling of the single D793E mutant. To investigate the possibility that this difference between VO_4 and BeFx may have been attributable to the trapping of ATP rather than ADP, we compared the photolabeling of wt and D793E dh of MRP1 under BeFx trapping conditions, using both azido-[γ-^{32}P]ATP and azido-[α-^{32}P]ATP (Figure 6B). The results of photolabeling with azido-[γ-^{32}P]ATP indicate that a significant portion of the nucleotide trapped at NBS1

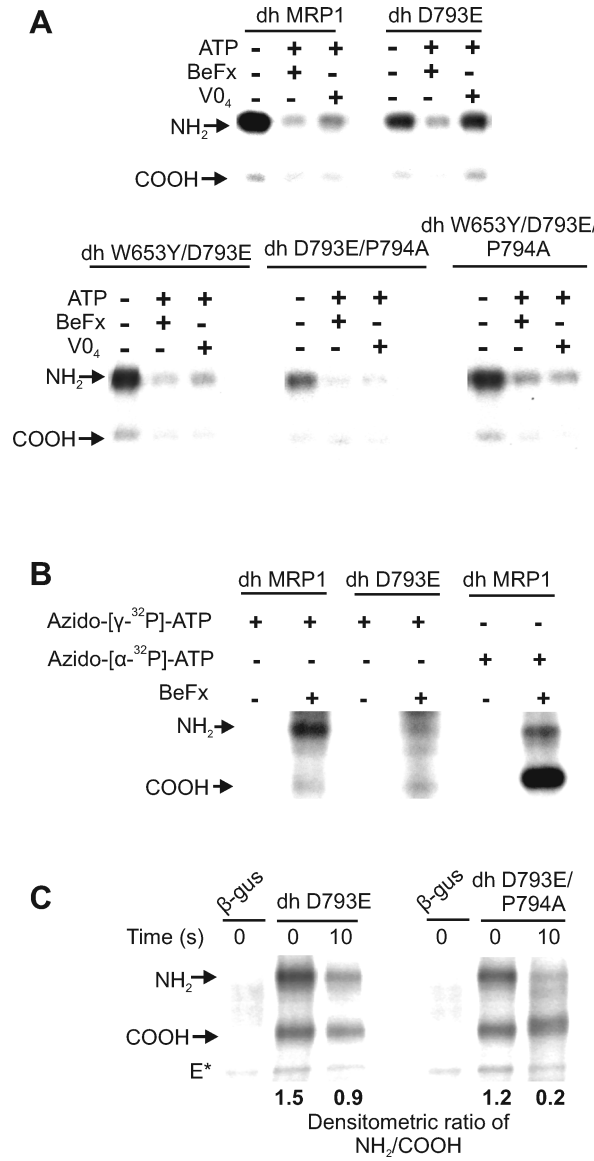

FIGURE 6: Photolabeling of wt and mutant dh of MRP1 with [^{3}H]LTC_4 and 8-azido-[^{32}P]ATP under hydrolytic conditions. (A) Membrane vesicles (50 μg of total protein) from Sf21 cells expressing wt dh of MRP1 and dh of various mutant proteins described in the text were incubated with [^{3}H]LTC_4 (200 nM, 200 nCi) at 23 °C for 20 min in the absence or presence of ATP (1 mM) plus BeFx (200 μM) or VO_4 (1 mM). UV cross-linking and SDS−PAGE of [^{3}H]LTC_4-labeled protein was performed as described in Materials and Methods. (B) Photolabeling of wt and D793E mutant dh of MRP1 with 8-azido-[γ-^{32}P]ATP or 8-azido-[α-^{32}P]ATP in the presence or absence of BeFx or VO_4. Membrane vesicles (20 μg of total protein) from Sf21 cells expressing wt or D793E dh of MRP1 were incubated with 8-azido-[γ-^{32}P]ATP or 8-azido-[α-^{32}P]ATP in the presence and absence of BeFx or VO_4 under trapping conditions, as described in Figure 5. (C) Sf21 membrane vesicles (50 μg of total protein) containing D793E or D793E/P794A dh of MRP1 were incubated with 8-azido-[α-^{32}P]ATP (15 μM) for 15 min at 37 °C. Samples were cooled to 20 °C, and aliquots (10 μL) were then snap-frozen either immediately prior to or 10 s after addition of ADP (final concentration 1.5 mM). Samples were then photo-cross-linked while frozen, washed to remove free nucleotides, and subjected to SDS−PAGE.

of wt MRP1 in the presence of BeFx is ATP rather than ADP. However, essentially no photolabeling of NBS1 of the D793E mutant was detected under similar conditions. This result is consistent with previous data indicating that the

tightly bound nucleotide present at NBS1 of this mutant is exclusively ADP (*26*).

In an attempt to directly compare the rate of release of ADP from NBS1 of the D793E and D793E/P794A mutants, both proteins were incubated with azido-[γ-^{32}P]ATP under hydrolytic conditions in the absence of VO_4 and BeFx. Aliquots were then snap-frozen and photo-cross-linked either immediately before or 10 s after the addition of a 100-fold molar excess of ADP (Figure 6C). The results indicated that prior to the addition of unlabeled ADP, the ratio of photolabeling of NH_2- and COOH-proximal NBDs of the single and double mutant proteins was 1.5 and 1.2, respectively. Within 10 s of addition of ADP, these ratios decreased to 0.9 and 0.2, respectively. The rapidity of the loss of nucleotide from NBD1 of the D793E/P794A mutant precluded determination of a time course of release. Nevertheless, the results are consistent with the P794A mutation increasing the rate of release of ADP from NBS1, as suggested by additional data presented above.

Effect of the P794A Mutation Alone on LTC_4 Transport, ATP Binding, and Nucleotide Trapping. Introduction of a W653Y mutation in wt MRP1 has been reported to have no detectable effect on ATP binding and hydrolysis (*49*). Consequently, we focused on the effect of the P794A mutation on the wt protein, both with respect to LTC_4 transport, as well as ATP binding and nucleotide trapping. The P794A mutation almost doubled LTC_4 transport relative to wt MRP1 (Figure 7B). However, the mutation had little effect on (i) ATP binding at 0 °C, as assessed by photolabeling with 8-azido-[γ-^{32}P]ATP (Figure 8A), (ii) VO_4- and BeFx-dependent nucleotide trapping (Figure 8B), and (iii) LTC_4 photolabeling in the absence of nucleotide or in the presence of ATP plus VO_4 or ATP plus BeFx (Figure 8C). However, the P794A mutation had a modest effect on the decrease in LTC_4 binding observed in the presence of ATP-γ-S (Figure 8C). Densitometry indicated that, in the presence of ATP-γ-S, photolabeling of the NH_2-terminal half of wt MRP1 decreased ~4-fold while labeling of the P794A mutant decreased only ~2-fold.

To further examine the underlying cause of the increase in transport activity resulting from the P794A mutation, we determined the ATP dependence of LTC_4 transport (Figure 9). The results of transport assays carried out with vesicles containing wt or P794A dh MRP1 at various concentrations of ATP indicated that the mutation did not affect the K_m(ATP), which was determined to be 59 μM for the wt protein and 62 μM for the P794A mutant. However, the mutation increased the normalized V_{max} for LTC_4 from 21 pmol·min^{-1} for the wt protein to 47 pmol·min^{-1} for the mutant.

Molecular Dynamics Modeling and Possible Mechanisms Underlying the Effects of the D793E and the Secondary D794A Mutations. Mutational studies of the bacterial ABC transporters, such as BmrA and MJ0796, revealed the catalytic importance of the Glu residue immediately following the Walker B (*50, 51*). In prokaryotic, ATP-bound NBD crystal structures such as GlcV-AMPPNP-Mg, this Glu residue accesses the γ-phosphate (γ-P) group of ATP *via* an activating water molecule (*52*). Unexpectedly, given the catalytic importance attributed to the carboxylate side chain of the Glu residue, a GlcV mutant containing Gln at this position retained approximately 20% of wt ATPase activity,

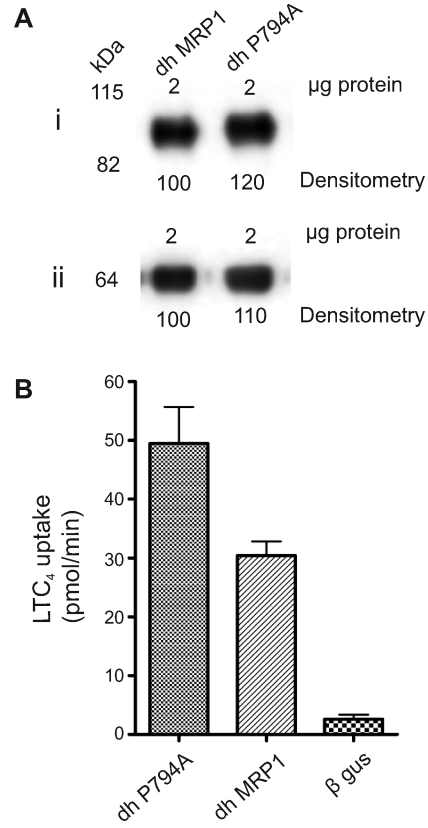

FIGURE 7: Comparison of [^{3}H]LTC_4 transport by wt dh MRP1 and dh MRP1P794A. (A) Membrane vesicle proteins from Sf21 cells (2 μg) expressing wt dh MRP1 or dh MRP1P794A or Sf21 cells infected with a control vector expressing β-gus were separated by SDS−PAGE using a 10% gel which was then immunoblotted; the NH_2 and COOH halves of the wt and mutant proteins were detected with mAbs MRPr1 (i) and MRPm6 (ii), respectively, and quantified by densitometry. Expression levels relative to wt dh MRP1 are indicated beneath each immunoblot. (B) Membrane vesicles (2 μg) containing wt dh MRP1 and dh MRP1P794A were assayed for [^{3}H]LTC_4 transport activity at 23 °C for 1 min in transport buffer (pH7.4) containing LTC_4 (50 nM, 20 nCi). The transport data from triplicate samples in a typical experiment were normalized based on relative levels of protein expression determined in panel A.

indicating that Glu is not universally essential for catalytic activity (*54*). The recent crystal structure of wt MRP1 NBD1, in which the catalytic Glu is replaced with Asp, indicates that the carboxyl side chain of D793 points away from the activating water molecule rather than toward it (*27*). In this study, we modeled the structure of an MRP1 NBD1/2 dimer as described previously (*27*) and mutated D793 to E to investigate the possible effect of this mutation on ATP hydrolysis. In this model, the Glu residue in the D793E mutant NBD1 forms a [carboxylate oxygen−hydrolytic water−ATP γ-P] catalytic dyad for ATP hydrolysis (Figure 10). The Glu carboxylate oxygen and the γ-phosphate of ATP are bridge-linked by a potentially hydrolytic water molecule that forms the H-bonds with both groups. In order for a stable catalytic dyad to form, the distance of the H-bond should be in the range of 2.5−3.5 Å, and the water-mediated distance between the carboxylate oxygen and ATP γ-P atom should be in the range of 5.0−7.0 Å. In our dynamics simulation analysis, the side chain of D793 in the wt NBD1 was relatively rigid, and most distance variations between D793 and ATP γ-P were >8.0 Å (8.0−11.0 Å, data not shown). Thus, the catalytic dyad cannot form readily. However, in the D793E mutant, the distance variation range

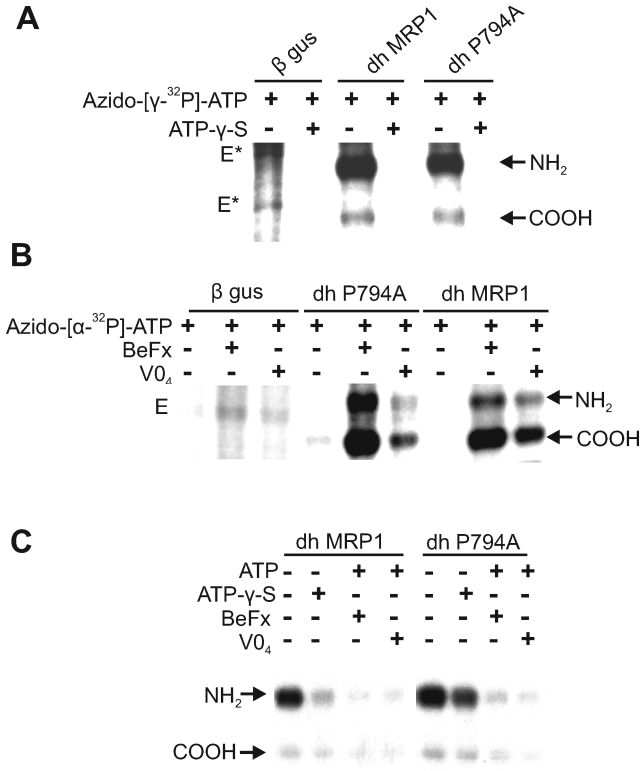

FIGURE 8: Photolabeling of wt dh MRP1 and dh MRP1P794A by 8-azido-[γ-^{32}P]ATP, 8-azido-[α-^{32}P]ATP, and [^{3}H]LTC$_4$. (A) Membrane vesicles (20 μg of total protein) from Sf21 cells expressing wt dh MRP1, dh MRP1P794A and control β-gus were incubated with 8-azido-[γ-^{32}P]ATP (5 μM) on ice for 5 min in the absence or presence of ATP-γ-S (500 μM). Samples were UV cross-linked, and unincorporated nucleotides were removed prior to separation of membrane proteins by SDS−PAGE and autoradiography to detect labeled proteins. (B) Membrane vesicles (20 μg of total protein) from the same preparations used in panel A were incubated with 8-azido-[α-^{32}P]ATP (10 μM) at 37 °C for 15 min in the absence or presence of BeFx (200 μM) or VO_4 (1 mM). After removing free nucleotide, the labeled samples were UV cross-linked, separated by SDS−PAGE using gradient gels, and autoradiographed to detect labeled proteins. (C) Membrane vesicles (50 μg of total protein) containing wt dh MRP1 or dh MRP1P794A were incubated with [^{3}H]LTC$_4$ (200 nM, 200 nCi) for 20 min at 23 °C in the absence or presence of ATP-γ-S (4 mM) or ATP (1 mM) plus BeFx (200 μM) or VO_4 (1 mM). Samples were then subjected to repeated cycles of freezing in liquid nitrogen and UV cross-linking. Membrane proteins from all samples were separated by SDS−PAGE on a single gradient gel, and [^{3}H]LTC$_4$ photolabeling was determined by autoradiography. (D) In (A)−(C), the positions of NH_2- and COOH-proximal halves of the wt and mutant proteins are indicated by NH_2 and COOH, respectively. Labeled endogenous proteins are indicated by E*.

between the carboxylate oxygen of E793 and the ATP γ-P atom was 5.5−12.0 Å, with more flexibility to form an effective catalytic dyad (data not shown). In Figure 10, a snapshot of the simulation is displayed showing the difference between the orientation of the Glu and Asp side chains at position 793. In the D793E mutant the distance between the carboxylate oxygen of E793 and the catalytic water hydrogen atom is approximately 2.74 Å, which is short enough to form a stable H-bond. However, in the native NBD1, the distance between the Asp carboxylate oxygen and the water hydrogen atom is 4.17 Å, making it unlikely for a stable hydrogen bond to be formed. This provides a plausible explanation for the increase in ATP hydrolysis at NBS1 resulting from the D793E mutation (*26*).

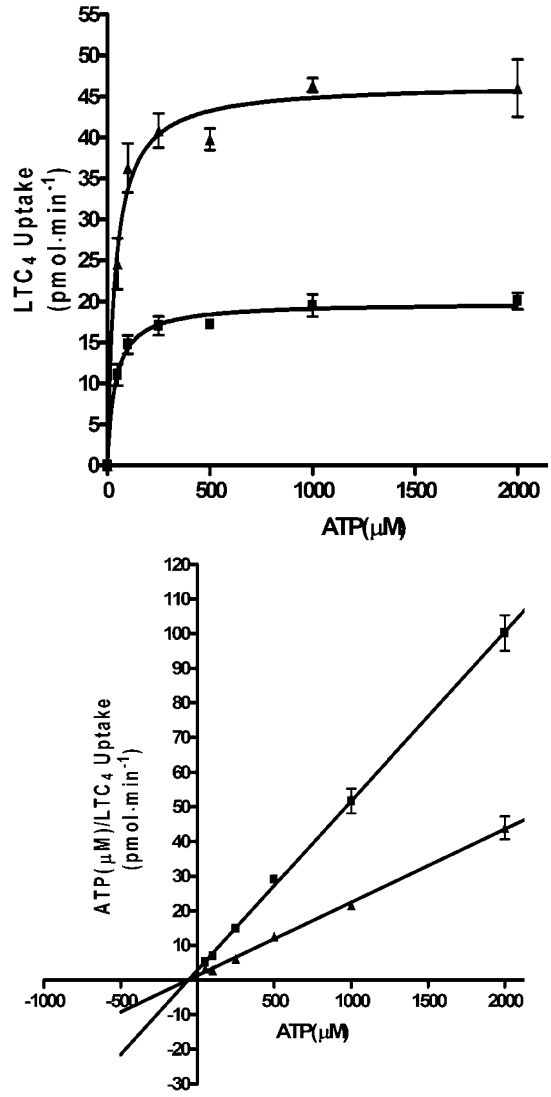

FIGURE 9: Determination of the effect of the P794A mutation on the ATP dependence of LTC$_4$ transport. LTC$_4$ transport by membrane vesicles (2 μg of total membrane protein) from Sf21 cells expressing wt dh MRP1 (■) or dh MRP1P794A (▲) was measured in the presence of various concentrations of ATP ranging from 50 μM to 2 mM at a fixed concentration of [^{3}H]LTC$_4$ (150 nM, 30 nCi) for 1 min at 23 °C (upper panel). K_m and V_{max} values were determined from a Hanes−Woolf transformation of the uptake data (lower panel).

Dynamic Simulation of ADP-Bound MRP1-NBD1 Suggests That the Additional P794A Mutation Affects ADP Binding through the Walker A Motif and the Q-Loop. In ATP-bound MRP1-NBD1 crystal structures, binding of ATP is stabilized by interactions with residues in the Walker A motif and the Q-loop. The β-phosphate group of ATP hydrogen bonds with the main-chain nitrogen atom of K684 and also tightly complexes the Mg^{2+} ion, which is coordinated by the amide oxygen of Q713 in the Q-loop (*27*). Similar ATP-binding interactions were also observed in other ABC-NBD structures, such as MJ0796 and HlyB (*24, 53*).

To perform dynamics simulation of ADP binding, we first substituted the ATP molecule with ADP in NBS1 of the NBD1/2 dimer structure and subjected the model to energy minimization as described. The modeling and dynamic simulation data suggest that in D793E MRP1 the ϵ-amino atom of K684 in the Walker A motif forms tight and stable H-bonds of ~3.0 Å with the β-phosphate oxygen, with the

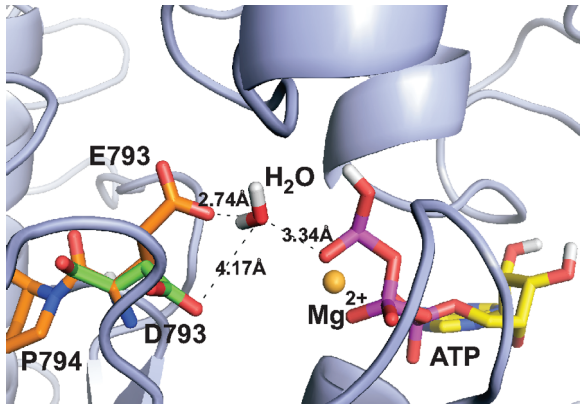

FIGURE 10: Predicted spatial relationships of ATP, Mg^{2+}, and the catalytic water molecule with P794, D793, and mutant E793 at NBS1. The figure, created using Pymol (http://www.pymol.org) from the NBD dimer model described in the text, shows the relative positions of the wt D793 and mutant E793 residues, illustrating the differences in the orientations of the carboxylate side chains and their distances from the catalytic water molecule.

distance between the K684 ϵ-amino nitrogen atom and ADP β-P_i in MRP1D793E varying between 4.0 and 5.5 Å (Figure 11A,C). In addition, Q713 in the Q-loop is extremely rigid, maintaining a constant distance of only ~2.0 Å between the side-chain δ-oxygen and the Mg^{2+} ion, thus further stabilizing ADP binding (Figure 11A,D). However, the additional P794A mutation eliminated the rigid, main-chain kink of P794. This results in an increase in the flexibility of the joint region between the Walker B motif and the D-loop, which in turn destabilizes interactions that contribute to the tight binding of ADP. The consequence of this flexible regional structure in the A794 mutant is reflected by the changing dynamics of the ADP-binding site. Thus in the D793E/P794A mutant, the variation in distances between the K684 ϵ-amino nitrogen atom and β-P_i is considerably increased compared to the D793E single mutation (Figure 11B,C). In addition, in D793E/P794A MRP1 the interaction between Q713 and the Mg^{2+} ion is also decreased with an abrupt fluctuation in distance from 2 to 6.0−8.0 Å occurring during a 40 ps dynamic simulation (Figure 11B,D). Since magnesium plays an important role in stabilizing the binding of ADP, the withdrawal of Q713 from Mg^{2+} would be expected to further destabilize ADP binding and to favor a more rapid release of ADP following ATP hydrolysis.

DISCUSSION

Efflux of substrate by ABC transporters such as the MRPs and P-gp is believed to involve ATP-dependent cycling of the protein between high- and low-affinity substrate binding states. There is compelling evidence that the switch from "inward facing", high-affinity to "outward facing", low-affinity conformations involves the cooperative binding of two ATP molecules (and possibly hydrolysis of one), resulting in formation of a "tight" NBD dimer (reviewed in refs *48* and *56*). The movement and conformational changes of the NBDs induced by ATP binding are thought to be transduced *via* cytoplasmic coupling loops to the MSDs resulting in a decrease in affinity for substrate (*55*). The precise mechanism involved in resetting the transporter in a high-affinity state is less well established but is believed to involve hydrolysis of at least one ATP molecule and the release of ADP, which is likely the rate-limiting step in the transport cycle.

In proteins with idntical or functionally interchangeable NBDs, initial binding of ATP may occur at either NBS, and there seems to be no apparent order in which the two bound ATP molecules are hydrolyzed (*56*). However, in MRP1 and possibly other related ABCC proteins where the NBDs are not functionally interchangeable, the switch from high- to low-affinity conformation appears to involve the sequential binding of ATP, first to NBS1 followed by binding and hydrolysis of ATP at NBS2 (*48*). It is less clear whether hydrolysis at NBD1 and release of ADP are a prerequisite for resetting MRP1 in a high-affinity conformation, and it has been questioned whether MRP1 is capable of hydrolyzing ATP at NBS1 because of the presence of Asp rather than a Glu residue at position 793 (*27, 48*). However, azido-ADP can be trapped by wt NBD1 in the presence of VO_4, albeit at a relatively low level compared with NBD2, suggesting that some hydrolysis can occur (Figure 5) (*26, 48*). Furthermore, the ATPase activity of purified MRP1 (0.015−0.03 s^{-1}) is approximately 100-fold lower than transporters with two typical NBDs, such as P-gp (*13, 57*). Recent studies of purified P-gp in which the "catalytic" Glu residues in both NBDs were mutated revealed that the mutant protein had a low but measurable ATPase activity of 0.012 s^{-1}, which is 40−80% of the rate estimated for purified MRP1 (*13, 57*). Overall, these observations leave open the possibility that the rate of ATP hydrolysis and ADP release from the atypical NBS1 of MRP1 may determine the overall ATPase and transport activity of the protein (*48*).

Previously, we demonstrated that reduced LTC_4 transport by MRP1D793E is associated with an impaired ability to release ADP from NBS1 (*26*). We also showed that this tight binding of ADP effectively locks the mutant protein in a high-affinity state and appears to be incompatible with formation of a tight NBD dimer (*26*). Thus, we hypothesized that ADP release from NBD1 was a possible rate-limiting step for entry of the mutant protein into another transport cycle. In this study we sought to test this hypothesis by searching for secondary mutations that would restore LTC_4 transport by MRP1D793E and examining their effect on the VO_4-independent tight binding of ADP by NBS1. We identified candidate residues based on evolutionary conservation of atypical amino acids in critical regions of NBD1 and NBD2 of the ABCC proteins and mutated them to those found in more typical ABC NBDs. Among the mutants tested, two secondary mutations, W653Y and P794A, increased LTC_4 transport activity of the D793E mutant to levels equal to or greater than that of the wt protein (Figure 3).

Neither of the W653Y or P794A mutations altered azido-ATP binding by MRP1D793E under nonhydrolytic conditions, but both decreased VO_4-independent tight binding of ADP at 37 °C by NBD1 (Figure 5). Thus the presence of Trp at position 653 and Pro at position 794 in MRP1 NBD1, rather than the typical Tyr and Ala, respectively, may contribute to the tight binding of ADP exhibited by MRP1D793E. Conversely, the Tyr and Ala residues present at the corresponding locations in more typical NBDs may be determinants of the rate of ADP release. Consistent with this suggestion, the W653Y and P794A mutations increased VO_4-dependent nucleotide trapping at NBS1 of MRP1D793E.

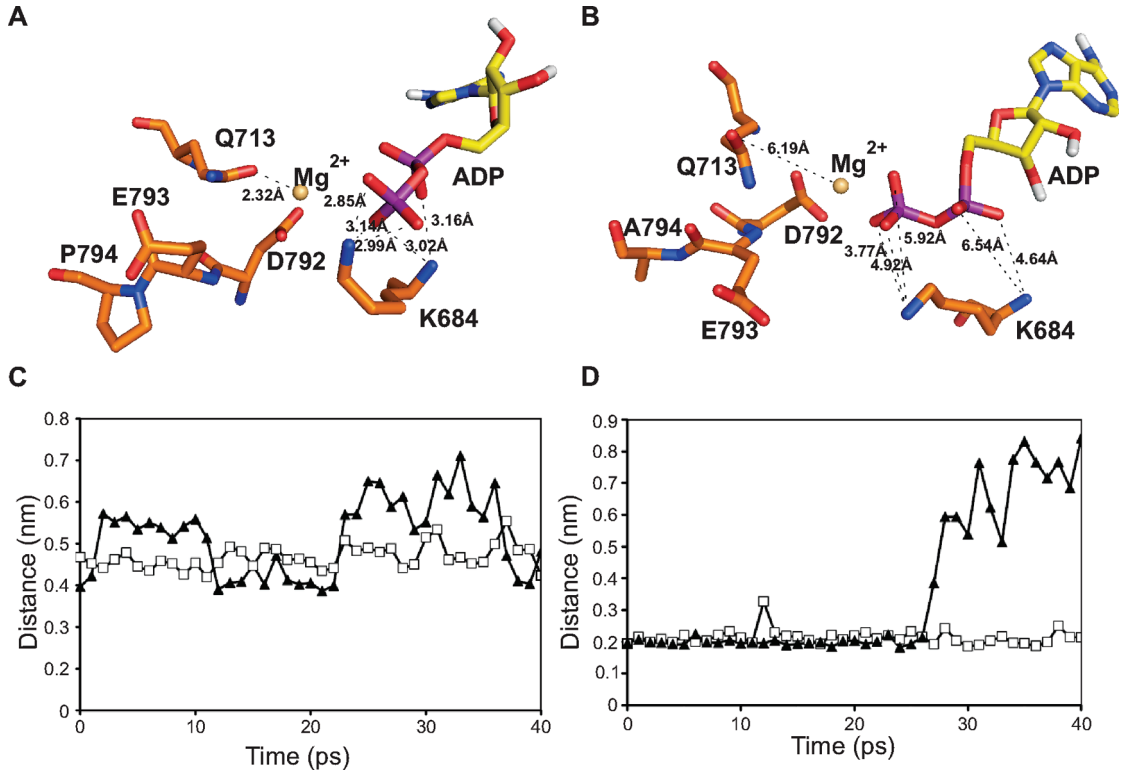

FIGURE 11: Molecular dynamics simulations of ADP binding at NBS1 of MRP1D793E and MRP1D793E/P794A. Panels A and B show the spatial relationship of selected key residues from NBD1 interacting with ADP and Mg^{2+} in MRP1D793E (A) and MRP1D793E/P794A (B). In MRP1D793E (panel A), the nitrogen atoms of K684 form multiple H-bonds (<3.3 Å) with oxygens of ADP phosphates, especially between the K684 ϵ-amino nitrogen and ADP β-phosphate. In addition, the Mg^{2+}ion is within interaction range of the δ-oxygen atom of Q713. In MRP1D793E/P794A (panel B), the ϵ-amino atom of K684 cannot form H-bonds with oxygens of the ADP β-phosphate, and the side chain of Q713 will "swing" away, thus weakening its bond to the Mg^{2+} ion. The numbers in Å represent the distances from the K684 ϵ-amino nitrogen to the ADP phosphate oxygens or from the δ-oxygen atom of Q713 to Mg^{2+}. In panel C, the dynamic distance between the K684 ϵ-amino nitrogen atom and ADP β-P_i in MRP1D793E (□) was compared to the equivalent distance in MRP1D793E/P794A (▲). Panel D shows a similar comparison of the distance between the Q713 δ-oxygen and the Mg^{2+} ion (MRP1D793E, □; MRP1D793E/P794A, ▲).

However, the extent of VO_4-dependent ADP trapping at NBS2 in the W653Y/D793E and P794A/D793E mutants was reduced relative to wt MRP1, as observed with the original D793E mutant (*26*). This is likely the consequence of increased ATP hydrolysis and VO_4-dependent trapping of ADP at NBS1 and, based on the alternating sites model of catalysis, the inability to trap ADP in a VO_4-dependent posthydrolytic transition state at both NBSs simultaneously (*26*). However, it should be noted that although Trp and Pro are highly conserved in NBD1 of the ABCC proteins, their presence is not invariably associated with low catalytic activity. Trp and Pro are found at the corresponding locations in the NBD of the *Escherichia coli* transporter, MalK, and Pro is present in the NBD of *Salmonella typhimurium* HisP (Figure 1), both of which have more typical levels of ATPase activity. Thus the effect of these amino acids on catalytic activity must be context dependent to some extent.

In contrast to VO_4, BeFx markedly increased trapping at NBS2 and modestly increased trapping at NBS1 of the D793E single mutant, so that the labeling profile of MRP1D793E was very similar to that of wt protein (Figure 5). Furthermore, the combination of BeFx and ATP also induced a shift from high- to low-affinity LTC_4 binding by MRP1D793E that was not seen in the presence of ATP plus VO_4. These results strongly suggest that in the presence of BeFx the conformation of nucleotide-bound NBS1 of the mutant protein, in contrast to the conformation formed in the absence of BeFx (or in the absence/presence of VO_4), is compatible with the formation of a closed NBD dimer (*45, 46, 48*). This difference in the effects of VO_4 and BeFx may reflect the different geometries required for each anion to stabilize nucleotide binding. Although not directly comparable, similar observations have been reported with P-gp mutants which are catalytically inactive by virtue of mutation of an essential Lys residue in one or other Walker A motif (*58*). Although these mutants display little or no ATPase activity and no VO_4-dependent trapping of ADP, they do trap nucleotide in the presence of BeFx or fluoroaluminate. As discussed below, stabilization of an early transition state by BeFx at NBS1 of MRP1D793E may be possible, while the VO_4 transition state may be energetically unfavorable compared with the tight binding of ADP which occurs in this mutant in the absence of stabilizing anion. It was hypothesized during studies of ATPase-deficient P-gp mutants that the nucleotide occluded in the presence of BeFx was ATP as opposed to ADP (*55*). However, we have confirmed that this is not so with the MRP1D793E mutant by comparing the results of trapping experiments using 8-azido-[γ-^{32}P]ATP and 8-azido-[α-^{32}P]ATP (Figure 6B) which revealed no trapping of radioactive nucleotide by either NBS when the γ-labeled isotope was used.

The functional importance of the aromatic residue at the position corresponding to W653 has been studied previously in several ABC transporters, including wt

MRP1 (*49*) and P-gp where the comparable residue is Y401 (*59*). W653 and its counterparts in other transporters reside in a subdomain of the NBD that has recently been termed the A-loop, and they have been shown to stabilize ATP binding by interacting with the adenine ring (*27, 59*−*61*). In the context of P-gp, mutation of Tyr to Trp was found to have no significant functional consequences, although mutation to a nonaromatic residue markedly destabilized ATP binding (*59, 60*). In wt MRP1, the converse mutation was reported to have no detectable effects on ATP binding or trapping. Nevertheless, it approximately doubled LTC_4 transport activity (*49*). These effects on transport are consistent with our observations with MRP1D793E, but our results strongly suggest that the increase in activity is attributable to an increase in the release of ADP from the D793E/W653Y mutant protein, that may not have been apparent from studies of wt MRP1. Thus the presence of Trp rather than Tyr may contribute to the significantly more stable interactions with ADP observed with the MRP1D793E mutant, possibly as a result of differences in the relative strength of $\beta-\beta$ interactions formed between the indole and phenolic side chains of the two aromatic residues and the adenine ring (*27*).

In contrast to W653, the role of P794 and the corresponding residues in other ABC transporters has not been described. Consequently, in addition to studying the effect of the P794A mutation on the function of MRP1D793E, we also generated this mutation in the wt protein. The mutation more than doubled the rate of LTC_4 transport by wt MRP1 protein but had little or no effect on nucleotide binding or trapping as assessed by photolabeling studies with azido-ATP. Nor did it significantly alter the ability to shift from high- to low-affinity LTC_4 binding states in the presence ATP plus VO_4 or BeFx, although it did cause a modest decrease in the ability of ATP-γ-S to affect such a shift.

We also assessed the effect of the P794A mutation on the apparent affinity for ATP by comparing the ATP dependence of LTC_4 transport by the P794A mutant and wt proteins. The results revealed that the mutation did not affect the K_m for ATP but doubled the V_{max} for LTC_4 transport, suggesting that it was affecting a step in the transport cycle subsequent to the initial binding of nucleotide. Combined with data derived from transport and photolabeling studies with azido-ATP and LTC_4, the results are consistent with the possibility that the Pro to Ala mutation increases the ability to release ADP from NBS1. This possibility is also strongly supported by direct comparison of the rapidity of the release of ADP from NBS1 of the D793E and D793E/P794A mutant proteins (Figure 6C).

To obtain more mechanistic insight into the effect of the P794A mutation on nucleotide binding, we also generated a model of the MRP1 NBD dimer and used a molecular dynamics approach to simulate the predicted effects of the Pro to Ala mutation on ADP binding by MRP1D793E. As in several crystal structures of ADP-bound NBDs, such as GlcV and MalK, binding of ADP by NBS1 in the MRP1 NBD dimer model is stabilized by direct interactions with the Walker A motif and the Q-loop (*52, 62*). Specifically in the case of MRP1, the β-phosphates of ATP and Mg^{2+} are predicted to interact with Walker A K684 and Q-loop Q713 residues, respectively (*27*). In MRPD793E, molecular dynamics simulation predicts that these interactions are both relatively stable and, in the case of Q713, extremely rigid. P794 is located at the joint between the Walker B motif and the D-loop and does not interact with ADP directly. Although P794 has no direct interaction with ADP, molecular dynamics simulation suggests that the identity of the residue at this position may have strong, long-distance effects on the stability of the interactions involving K684 and Q713.

The rigidity of the D-loop conferred by Pro794 appears to contribute to the stability of the interactions between ADP and K684 and between Q713 and Mg^{2+}. The increase in flexibility resulting from the replacement of Pro with Ala enables K684 to swing away from the β-phosphate of ADP and Q713 to move more readily away from Mg^{2+} (Figure 10). With this increase in flexibility, the residence time of the side chains of both residues outside of the range necessary to form stable interactions is predicted to increase, which in turn would be expected to enhance the rate of release of ADP from NBS1. Overall, the experimental results of this and previous studies, combined with molecular dynamics simulations, strongly suggest that ATP hydrolysis occurs at NBS1, albeit with low efficiency, and that ADP release from this site, at least in the D793E mutant protein, may be rate limiting in the transport cycle of MRP1.

ACKNOWLEDGMENT

The authors thank Monika Vasa and Ruth Burtch-Wright for excellent technical assistance and Maureen Hobbs for preparation of the manuscript. We also acknowledge Dr. Shiu-Pang Tam for critical reading of the manuscript and for contributions to certain nucleotide photolabeling studies of MRP1.

REFERENCES

1. Deeley, R. G., and Cole, S. P. C. (2003) Multidrug resistance protein 1 (ABCC1), in *ABC Proteins: From Bacteria to Man*, Chapter 19, pp 393−422, Academic Press Elsevier Science, London.
2. Cole, S. P. C., and Deeley, R. G. (1998) Multidrug resistance mediated by the ATP-binding cassette transporter protein, MRP. *BioEssays 20*, 931–940.
3. Cole, S. P. C., Bhardwaj, G., Gerlach, J. H., Mackie, J. E., Grant, C. E., Almquist, K. C., Stewart, A. J., Kurz, E. U., Duncan, A. M., and Deeley, R. G. (1992) Overexpression of a transporter gene in a multidrug resistant human lung cancer cell line. *Science 258*, 1650–1654.
4. Kool, M., de, H. M., Scheffer, G. L., Scheper, R. J., van Eijk, M. J., Juijn, J. A., Baas, F., and Borst, P. (1997) Analysis of expression of cMOAT (MRP2), MRP3, MRP4, and MRP5, homologues of the multidrug resistance-associated protein gene (MRP1), in human cancer cell lines. *Cancer Res. 57*, 3537–3547.
5. Kool, M., van der, L. M., de, H. M., Baas, F., and Borst, P. (1999) Expression of human MRP6, a homologue of the multidrug resistance protein gene MRP1, in tissues and cancer cells. *Cancer Res. 59*, 175–182.
6. Hopper, E., Belinsky, M. G., Zeng, H., Tosolini, A., Testa, J. R., and Kruh, G. D. (2001) Analysis of the structure and expression pattern of MRP7 (ABCC10), a new member of the MRP subfamily. *Cancer Lett. 162*, 181–191.
7. Bera, T. K., Lee, S., Salvatore, G., Lee, B., and Pastan, I. (2001) MRP8, a new member of ABC transporter superfamily, identified by EST database mining and gene prediction program, is highly expressed in breast cancer. *Mol. Med. 7*, 509–516.
8. Bera, T. K., Iavarone, C., Kumar, V., Lee, S., Lee, B., and Pastan, I. (2002) MRP9, an unusual truncated member of the ABC

transporter superfamily, is highly expressed in breast cancer. *Proc. Natl. Acad. Sci. U.S.A. 99*, 6997–7002.
9. Gao, M., Cui, H. R., Loe, D. W., Grant, C. E., Almquist, K. C., Cole, S. P. C., and Deeley, R. G. (2000) Comparison of the functional characteristics of the nucleotide binding domains of multidrug resistance protein 1. *J. Biol. Chem. 275*, 13098–13108.
10. Hou, Y., Cui, L., Riordan, J. R., and Chang, X. (2000) Allosteric interactions between the two non-equivalent nucleotide binding domains of multidrug resistance protein MRP1. *J. Biol. Chem. 275*, 20280–20287.
11. Nagata, K., Nishitani, M., Matsuo, M., Kioka, N., Amachi, T., and Ueda, K. (2000) Nonequivalent nucleotide trapping in the two nucleotide binding folds of the human multidrug resistance protein MRP1. *J. Biol. Chem. 275*, 17626–17630.
12. Hagmann, W., Nies, A. T., Konig, J., Frey, M., Zentgraf, H., and Keppler, D. (1999) Purification of the human apical conjugate export pump MRP2 reconstitution and functional characterization as substrate-stimulated ATPase. *Eur. J. Biochem. 265*, 281–289.
13. Mao, Q., Leslie, E. M., Deeley, R. G., and Cole, S. P. C. (1999) ATPase activity of purified and reconstituted multidrug resistance protein MRP1 from drug-selected H69AR cells. *Biochim. Biophys. Acta 1461*, 69–82.
14. Li, C., Ramjeesingh, M., Wang, W., Garami, E., Hewryk, M., Lee, D., Rommens, J. M., Galley, K., and Bear, C. E. (1996) ATPase activity of the cystic fibrosis transmembrane conductance regulator. *J. Biol. Chem. 271*, 28463–28468.
15. Beaudet, L., and Gros, P. (1995) Functional dissection of P-glycoprotein nucleotide-binding domains in chimeric and mutant proteins. Modulation of drug resistance profiles. *J. Biol. Chem. 270*, 17159–17170.
16. Hrycyna, C. A., Ramachandra, M., Germann, U. A., Cheng, P. W., Pastan, I., and Gottesman, M. M. (1999) Both ATP sites of human P-glycoprotein are essential but not symmetric. *Biochemistry 38*, 13887–13899.
17. Jones, P. M., and George, A. M. (2004) The ABC transporter structure and mechanism: perspectives on recent research. *Cell. Mol. Life Sci. 61*, 682–699.
18. Oswald, C., Holland, I. B., and Schmitt, L. (2006) The motor domains of ABC-transporters. What can structures tell us? *Naunyn Schmiedeberg's Arch. Pharmacol. 372*, 385–399.
19. Hopfner, K. P., Karcher, A., Shin, D. S., Craig, L., Arthur, L. M., Carney, J. P., and Tainer, J. A. (2000) Structural biology of Rad50 ATPase: ATP-driven conformational control in DNA double-strand break repair and the ABC-ATPase superfamily. *Cell 101*, 789–800.
20. Locher, K. P., Lee, A. T., and Rees, D. C. (2002) The E. coli BtuCD structure: a framework for ABC transporter architecture and mechanism. *Science 296*, 1091–1098.
21. Dawson, R. J. P., and Locher, K. P. (2006) Structure of a bacterial multidrug ABC transporter. *Nature 443*, 180–185.
22. Smith, P. C., Karpowich, N., Millen, L., Moody, J. E., Rosen, J., Thomas, P. J., and Hunt, J. F. (2002) ATP binding to the motor domain from an ABC transporter drives formation of a nucleotide sandwich dimer. *Mol. Cell 10*, 139–149.
23. Chen, J., Lu, G., Lin, J., Davidson, A. L., and Quiocho, F. A. (2003) A tweezers-like motion of the ATP-binding cassette dimer in an ABC transport cycle. *Mol. Cell 12*, 651–661.
24. Zaitseva, J., Jenewein, S., Jumpertz, T., Holland, I. B., and Schmitt, L. (2005) H662 is the linchpin of ATP hydrolysis in the nucleotide-binding domain of the ABC transporter HlyB. *EMBO J. 24*, 1901–1910.
25. Senior, A. E., al-Shawi, M. K., and Urbatsch, I. L. (1995) The catalytic cycle of P-glycoprotein. *FEBS Lett. 377*, 285–289.
26. Payen, L. F., Gao, M., Westlake, C. J., Cole, S. P. C., and Deeley, R. G. (2003) Role of carboxylate residues adjacent to the conserved core Walker B motifs in the catalytic cycle of multidrug resistance protein 1 (ABCC1). *J. Biol. Chem. 278*, 38537–38547.
27. Ramaen, O., Leulliot, N., Sizun, C., Ulryck, N., Pamlard, O., Lallemand, J. Y., Tilbeurgh, H., and Jacquet, E. (2006) Structure of the human multidrug resistance protein 1 nucleotide binding domain 1 bound to Mg^{2+}/ATP reveals a non-productive catalytic site. *J. Mol. Biol. 359*, 940–949.
28. Thompson, J. D., Higgins, D. G., and Gibson, T. J. (1994) CLUSTAL W: improving the sensitivity of progressive multiple sequence alignment through sequence weighting, position-specific gap penalties and weight matrix choice. *Nucleic Acids Res. 22*, 4673–4680.
29. Eddy, S. R. (1998) Profile hidden Markov models. *Bioinformatics 14*, 755–763.
30. Schuster-Bockler, B., Schultz, J., and Rahmann, S. (2004) HMM Logos for visualization of protein families. *BMC Bioinformatics 5*, 7.
31. Gao, M., Loe, D. W., Grant, C. E., Cole, S. P. C., and Deeley, R. G. (1996) Reconstitution of ATP-dependent leukotriene C_4 transport by co-expression of both half-molecules of human multidrug resistance protein in insect cells. *J. Biol. Chem. 271*, 27782–27787.
32. Gao, M., Yamazaki, M., Loe, D. W., Westlake, C. J., Grant, C. E., Cole, S. P. C., and Deeley, R. G. (1998) Multidrug resistance protein. Identification of regions required for active transport of leukotriene C_4. *J. Biol. Chem. 273*, 10733–10740.
33. Loe, D. W., Almquist, K. C., Deeley, R. G., and Cole, S. P. C. (1996) Multidrug resistance protein (MRP)-mediated transport of leukotriene C_4 and chemotherapeutic agents in membrane vesicles. Demonstration of glutathione-dependent vincristine transport. *J. Biol. Chem. 271*, 9675–9682.
34. Leier, I., Jedlitschky, G., Buchholz, U., Cole, S. P. C., Deeley, R. G., and Keppler, D. (1994) The MRP gene encodes an ATP-dependent export pump for leukotriene C_4 and structurally related conjugates. *J. Biol. Chem. 269*, 27807–27810.
35. Flens, M. J., Izquierdo, M. A., Scheffer, G. L., Fritz, J. M., Meijer, C. J., Scheper, R. J., and Zaman, G. J. (1994) Immunochemical detection of the multidrug resistance-associated protein MRP in human multidrug-resistant tumor cells by monoclonal antibodies. *Cancer Res. 54*, 4557–4563.
36. Hipfner, D. R., Gao, M., Scheffer, G., Scheper, R. J., Deeley, R. G., and Cole, S. P. C. (1998) Epitope mapping of monoclonal antibodies specific for the 190-kDa multidrug resistance protein (MRP). *Br. J. Cancer 78*, 1134–1140.
37. Qian, Y. M., Qiu, W., Gao, M., Westlake, C. J., Cole, S. P. C., and Deeley, R. G. (2001) Characterization of binding of leukotriene C_4 by human multidrug resistance protein 1: evidence of differential interactions with NH2- and COOH-proximal halves of the protein. *J. Biol. Chem. 276*, 38636–38644.
38. Payen, L., Gao, M., Westlake, C., Theis, A., Cole, S. P. C., and Deeley, R. G. (2005) Functional interactions between nucleotide binding domains and leukotriene C4 binding sites of multidrug resistance protein 1 (ABCC1). *Mol. Pharmacol. 67* 1944–1953.
39. Guex, N., and Peitsch, M. C. (1997) SWISS-MODEL and the Swiss-PdbViewer: an environment for comparative protein modeling. *Electrophoresis 18*, 2714–2723.
40. Schwede, T., Kopp, J., Guex, N., and Peitsch, M. C. (2003) SWISS-MODEL: An automated protein homology-modeling server. *Nucleic Acids Res. 31*, 3381–3385.
41. McRee, D. E. (1999) XtalView/Xfit—A versatile program for manipulating atomic coordinates and electron density. *J. Struct. Biol. 125*, 156–165.
42. Kutzner, C., van der, S. D., Fechner, M., Lindahl, E., Schmitt, U. W., de Groot, B. L., and Grubmuller, H. (2007) Speeding up parallel GROMACS on high-latency networks. *J. Comput. Chem. 28*, 2075–2084.
43. DeLano, W. L. (2002) The PyMOL Molecular Graphics System, DeLano Scientific, Palo Alto, CA.
44. Ramaen, O., Masscheleyn, S., Duffieux, F., Pamlard, O., Oberkampf, M., Lallemand, J. Y., Stoven, V., and Jacquet, E. (2003) Biochemical characterization and NMR studies of the nucleotide-binding domain 1 of multidrug-resistance-associated protein 1: evidence for interaction between ATP and Trp653. *Biochem. J. 376*, 749–756.
45. Urbatsch, I. L., Sankaran, B., Weber, J., and Senior, A. E. (1995) P-glycoprotein is stably inhibited by vanadate-induced trapping of nucleotide at a single catalytic site. *J. Biol. Chem. 270*, 19383–19390.
46. Senior, A. E., al-Shawi, M. K., and Urbatsch, I. L. (1995) The catalytic cycle of P-glycoprotein. *FEBS Lett. 377*, 285–289.
47. Fisher, A. J., Smith, C. A., Thoden, J. B., Smith, R., Sutoh, K., Holden, H. M., and Rayment, I. (1995) X-ray structures of the myosin motor domain of Dictyostelium discoideum complexed with MgADP·BeFx and MgADP·AlF_4^-. *Biochemistry 34*, 8960–8972.
48. Deeley, R. G., Westlake, C., and Cole, S. P. C. (2006) Transmembrane transport of endo- and xenobiotics by mammalian ATP-binding cassette multidrug resistance proteins. *Physiol. Rev. 86*, 849–899.
49. Zhao, Q., and Chang, X. B. (2004) Mutation of the aromatic amino acid interacting with adenine moiety of ATP to a polar residue alters the properties of multidrug resistance protein 1. *J. Biol. Chem. 279*, 48505–48512.

50. Moody, J. E., Millen, L., Binns, D., Hunt, J. F., and Thomas, P. J. (2002) Cooperative, ATP-dependent association of the nucleotide binding cassettes during the catalytic cycle of ATP-binding cassette transporters. *J. Biol. Chem. 277*, 21111–21114.
51. Orelle, C., Dalmas, O., Gros, P., Di, P. A., and Jault, J. M. (2003) The conserved glutamate residue adjacent to the Walker-B motif is the catalytic base for ATP hydrolysis in the ATP-binding cassette transporter BmrA. *J. Biol. Chem. 278*, 47002–47008.
52. Verdon, G., Albers, S. V., Dijkstra, B. W., Driessen, A. J., and Thunnissen, A. M. (2003) Crystal structures of the ATPase subunit of the glucose ABC transporter from Sulfolobus solfataricus: nucleotide-free and nucleotide-bound conformations. *J. Mol. Biol. 330*, 343–358.
53. Yuan, Y. R., Blecker, S., Martsinkevich, O., Millen, L., Thomas, P. J., and Hunt, J. F. (2001) The crystal structure of the MJ0796 ATP-binding cassette. Implications for the structural consequences of ATP hydrolysis in the active site of an ABC transporter. *J. Biol. Chem. 276*, 32313–32321.
54. Verdon, G., Albers, S.-V., van Oosterwijk, N., Dijkstra, B. W., Driessen, A. J. M., and Thunnissen, A.-M. W. H. (2003) Formation of the productive ATP-Mg21-bound dimer of GlcV, an ABC-ATPase from Sulfolobus solfataricus. *J. Mol. Biol. 334*, 255–267.
55. Locher, K. P. (2004) Structure and mechanism of ABC transporters. *Curr. Opin. Struct. Biol. 14*, 426–431.
56. Higgins, C. F., and Linton, K. J. (2004) The ATP switch model for ABC transporters. *Nat. Struct. Mol. Biol. 11*, 918–926.
57. Tombline, G., and Senior, A. E. (2005) The occluded nucleotide conformation of P-glycoprotein. *J. Bioenerg. Biomembr. 37*, 497–500.
58. Szakacs, G., Ozvegy, C., Bakos, E., Sarkadi, B., and Varadi, A. (2000) Transition-state formation in ATPase-negative mutants of human MDR1 protein. *Biochem. Biophys. Res. Commun. 276*, 1314–1319.
59. Ambudkar, S. V., Kim, I. W., Xia, D., and Sauna, Z. E. (2006) The A-loop, a novel conserved aromatic acid subdomain upstream of the Walker A motif in ABC transporters, is critical for ATP binding. *FEBS Lett. 580*, 1049–1055.
60. Kim, I. W., Peng, X. H., Sauna, Z. E., FitzGerald, P. C., Xia, D., Muller, M., Nandigama, K., and Ambudkar, S. V. (2006) The conserved tyrosine residues 401 and 1044 in ATP sites of human P-glycoprotein are critical for ATP binding and hydrolysis: evidence for a conserved subdomain, the A-loop in the ATP-binding cassette. *Biochemistry 45*, 7605–7616.
61. Zhou, Z., Wang, X., Liu, H. Y., Zou, X., Li, M., and Hwang, T. C. (2006) The two ATP binding sites of cystic fibrosis transmembrane conductance regulator (CFTR) play distinct roles in gating kinetics and energetics. *J. Gen. Physiol. 128*, 413–422.
62. Lu, G., Westbrooks, J. M., Davidson, A. L., and Chen, J. (2005) ATP hydrolysis is required to reset the ATP-binding cassette dimer into the resting-state conformation. *Proc. Natl. Acad. Sci. U.S.A. 102*, 17969–17974.

BI801532G